Available online at www.sciencedirect.com

ScienceDirect

Procedia Structural Integrity 53 (2024) 65–73

Structural Integrity Procedia

www.elsevier.com/locate/procedia

Third European Conference on the Structural Integrity of Additively Manufactures Materials (ESIAM23)

Production and characterization of lattice samples with solid shell in 17-4 PH stainless steel by Laser Powder Bed Fusion technology

Francesco Cantaboni[a]*, Marialaura Tocci[a], Paola S. Ginestra[a], Annalisa Pola[a], Elisabetta Ceretti[a]

[a]*Department of mechanical and industrial engineering, University of Brescia, Via Branze 38, 25123 Brescia, Italy.*

Abstract

In this work, 17-4 PH stainless steel square-based lattice structures with solid shell were manufactured by Laser Powder Bed Fusion. Face Centered Cubic unit cell was chosen as lattice cell geometry. The main aim of this work was to study the role of the shell in the mechanical behavior under compression load and to identify any critical issue due to the connection of the shell with lattice part. This is a relevant topic since often lattice structure are integrated with solid walls and the study of the relative behavior can support the understating of the performance of complex components. The manufactured samples were tested in as-built and heat-treated condition. In detail, solution and aging treatment was performed as a conventional route for 17-4PH steel. In particular, microhardness and compressive tests were performed, and the mechanical behavior and the fracture mechanisms of the samples were investigated. Furthermore, the defects, the geometry of the struts and the connection with the solid part were analyzed.
The detachment of the shell from the lattice did not occur. In fact, the solid part followed the deformation of the structure. The microstructural evolution after heat treatment was found to be responsible for an increase in hardness, strength and deformation for the investigated structures.

Keywords: L-PBF; 17-4PH; lattice structures; microstructure; mechanical characterization

*Francesco Cantaboni. Tel.: +39 348 516 0582
E-mail address: f.cantaboni@unibs.it

10.1016/j.prostr.2024.01.009

1. Introducion

Laser powder bed fusion (L-PBF) is the most common Additive Manufacturing (AM) process for the production of metallic components. Various alloys can be used, such as stainless steel, titanium, copper, aluminum, and cobalt alloys Bayat et al. (2019); Ginestra et al. (2020); Razavi et al. (2021). In particular 17-4 PH is usually used for the fabrication of stainless-steel parts due to its excellent weldability, corrosion resistance, high strength and hardness Cantaboni et al. (2022); Kareem et al. (2023); Leo et al. (2021). AM is used for the production of components with complex geometry with desirable mechanical properties, such as stochastic foams and lattice structures Bai et al. (2021); Bertocco et al. (2022). In particular, the lattice structures are widely used in aerospace, automotive and medical industry due to their excellent properties including lightweight, high strength and stiffness, heat dissipation and shock absorption Xiao et al. (2018).

The lattice structures are commonly used combined with fully dense structures and supports, as shown in the literature. For instance, the solid-lattice hybrid structures composed by solid and lattice part were already studied Dong et al. (2020a). In this work, a designed model of solid hybrid lattice structure, with optimized strut thickness connected to the solid part with Boolean operation, was proposed and compared with pure solid structure and a pure lattice structure. The authors demonstrated that the solid lattice hybrid structure shows the best mechanical performance. Moreover, the lattice structures are integrated in already existing components for weight reduction maintaining equivalent mechanical properties Bertol et al. (2010).

There are some studies where solid-lattice structures are tested to investigate the behavior between solid and lattice part. Jin F. et al. Fu et al. (2022) produced stainless steel 316L Triply periodic minimal surfaces (TPMS) shell lattices with different shell thicknesses. They proved that with increasing relative density, the deformation mechanism transforms from localized collapse to homogeneous bulk deformation showing the highest potential for lightweight designs. Moreover, G. Dong et al. Dong et al. (2020b) manufactured a hybrid element model defined by solid-lattice interface used to simulate the mechanical performance and optimize the material distribution of the lattice structure. The stiffness and the ultimate strength of the hybrid structure were higher than the solid and lattice structure separately.

In this work, square-based 17-4 PH samples with solid shell were produced by L-PBF technology, half of which were heat treated. The main aim of this work was to study the role of the shell in the mechanical behavior of complex structures under compression load and to identify eventual critical issues due to the connection of the shell with the lattice part.

Fig. 1. (a) square-based lattice sample with solid shell; (b) design of Face Centered Cubic (FCC) unit cell.

2. Materials and methods

2.1. Samples productions and heat treatment

Six square-based lattice samples with solid shell (as shown in Figure 1a) were designed and produced. The dimension of the samples is 22 (L) x 22 (L) x 20 (H) mm, where L and H are the length and the heigh of the structure, respectively. The thickness of the shell is 1 mm. The samples are characterized by a Face Centered Cubic (FCC) unit cell reported in Fig.1b with a length of 5 mm. The cylindrical struts with diameter (Dc) of 500 μm are connected to a

spherical node with a diameter (Dn) of 1.0 mm. Moreover, four bulk cubic samples with a length of 10 mm were produced for microstructural characterization and hardness measurements.

ProX® DMP 100 printer (3D system®, Wilsonville, Oregon, USA) was used to produce the samples in a controlled nitrogen inert gas atmosphere (O_2 < 0.01 %) with the process parameters reported in Table 1. Samples were designed using 3D XPert software, (ProX® DMP 100, 3D system, Rock Hill, South Carolina, USA).

Table 1. Process parameters used to produce the investigated samples.

Process Parameters	Value
Power [W]	100
Scanning speed [mm/s]	300
Hatch spacing [μm]	50
Layer thickness [μm]	30
Spot diameter [μm]	80

The samples were manufactured using 17-4 PH powder produced by LaserForm®, whose nominal chemical composition is reported in Table 2.

Table 2. Nominal chemical composition (wt%) of 17-4 PH powders used for the production of samples.

ELEMENT	Cr	Ni	Cu	Nb+Ta	C	Mn	P	S	Si	Fe
Wt. %	15.00 – 17.50	3.00 – 5.00	3.00 – 5.00	0.15 – 0.45	<0.07	<1.00	<0.04	<0.03	<0.01	Bal.

To enhance the mechanical properties of L-PBF 17-4 PH, half of the samples and two cubes were heat treated. The solution and aging treatments were performed on three samples using a furnace for vacuum heat treatment in order to achieve homogenization and effective precipitation-hardening An et al. (2023); Mahmoudi et al. (2017). During vacuum treatment a partial pressure of inert gas (Argon) was introduced in the furnace chamber. The samples were solution-treated at 1040 °C (T_1) for 1 h followed by cooling in argon flow with a pressure of 5 bar. The cooling rate was 80 °C/min. After solution treatment the samples were aged at 480 °C (T_2) for 4 h and cooled in air. The samples after heat treatment are named Heat Treated (HT) samples, while samples tested in as-built condition are indicated as AB.

2.2. Metallurgical, technological, and mechanical characterizations

Once manufactured, the height and length of the samples were measured with Vernier caliper and compared with the designed one. One AB sample was cut with a metallographic saw in order to observe a vertical and horizontal cross section and identify defects at the interface between lattice and shell and to perform a dimensional analysis of the structure. AB and HT (bulk) cubic samples were then mounted in acrylic resin, polished up to mirror finishing, and etched for 30 seconds with Fry's reagent to identify the main microstructural features.

The optical microscope (LEICA DMI 5000 M, Wetzlar, Germany) was used to measure strut diameter, shell thickness, porosity, and eventual defects at the connection between the lattice and solid shell. Furthermore, a deep analysis of the microstructure of samples were carried out under scanning electron microscope (SEM), LEO EVO® 40 (Carl Zeiss AG, Italy) equipped with Energy-Dispersive X-ray Spectroscopy (EDS) detector.

Moreover, Vickers microhardness measurements were performed with Mitutoyo HM-200 (Mitutoyo Corporation, Kawasaki (Kanagawa, Japan) hardness testing machine on four cubic samples (two of which treated) to evaluate the effectiveness of the heat treatment. A load of 0.5 kg was applied for 15 s. Ten repetitions for each condition were performed along the cross section.

Compressions tests were carried out with a servo-hydraulic testing machine Galdabini QUASAR 250 (Galdabini (S.P.A.), Cardano Al Campo VA, Italy) equipped with a 250 kN load cell. The tests were conducted in displacement

control at a constant crosshead velocity of 2 mm/min and the displacement was measured using the crosshead movement. The stress-strain curves were obtained, and the mechanical features were calculated, such as Young's modulus, yield stress (as compressive offset stress at the plastic compressive strain of 0.2 %) and ultimate strength (as the peak of stress detected). The failure of the samples was analyzed.

3. Results and discussion

3.1. Samples characterizations

The samples length and height, the thickness (tk) of the solid shell and the diameter (Dc) of the struts were measured on the cross section of the lattice specimens and the results are reported in Table 3. It has to be mentioned that the height of samples was slightly influenced by the support removal.

The diameter of the struts resulted close to the designed one (0.5 mm), while the thickness of the shell was below the design value (1.0 mm). The calculated standard deviation is reasonable, meaning a regular geometric size. The thickness of the shell resulted slightly lower than the design and this was probably due to the instability of the process and thermal distortion in consequence of the laser scan strategy and the use of low-energy settings Wu, Narra, and Rollett (n.d.).

Table 3. Measured dimensions of As-Built samples.

H [mm]	L [mm]	Dc [µm]	tk [µm]
19.1 ± 0.16	21.98 ± 0.05	508.1 ± 34.1	930.4 ± 18.4

The interface between lattice and solid part is known to represent a critical feature and was therefore analyzed. In Figure 2, two micrographs of the connection between lattice and shell were reported as representative examples. In particular, in Fig. 2a a critical connection is shown. In this case, lack-of-fusion porosities were detected on the connection between strut and node, sensibly reducing the load bearing area. On the other hand, as shown in Fig. 2b, often the connections were denser, with smaller porosities. In both cases the junction between node and shell was denser than the strut-node connections. The critical features were probably due to the local lack of melting and the abrupt change of geometry from thin struts to a bulk structure.

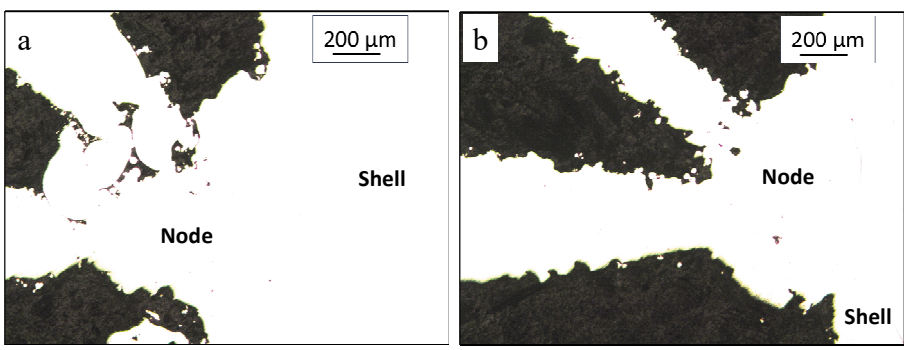

Fig. 2. Two examples of connection between lattice and shell. (a) lack-of-fusion porosities and (b) denser connection with small porosities.

3.2. Microstructure

The micrographs of the longitudinal (L) and transverse (T) cross-section of as-built 17-4 PH samples were reported in Fig. 3a and 3b, respectively.

The typical microstructure of 17-4 PH alloy produced by L-PBF is clearly visible. The presence of partially overlapped melt pools, formed due to the melting of metal powders under the laser action, is highlighted by the white arrows on the L cross section in Figure 3a. The scan tracks identifying the path of the laser during the manufacturing

process are highlighted by yellow arrows on the T cross section in Fig. 3b, as in accordance with C. Garcia-Cabezon et al. (2022). Moreover, the typical sections of the columnar grains are visible in Fig. 3b.

The HT samples show a completely different microstructure, as reported in Fig. 3c and 3d. The melt pools and scan tracks disappeared due to the solution treatment An et al. (2023b). Black dots are also visible on both cross sections after heat treatment. These are likely precipitates formed during aging treatment. These appears to be present along the grain boundaries but also dispersed in the matrix.

Moreover, during the manufacturing process the presence of nitrogen as an austenite-stabilizing element likely allowed the formation of austenite which is only partially transformed into martensite during rapid solidification cooling Leo et al. (2021).

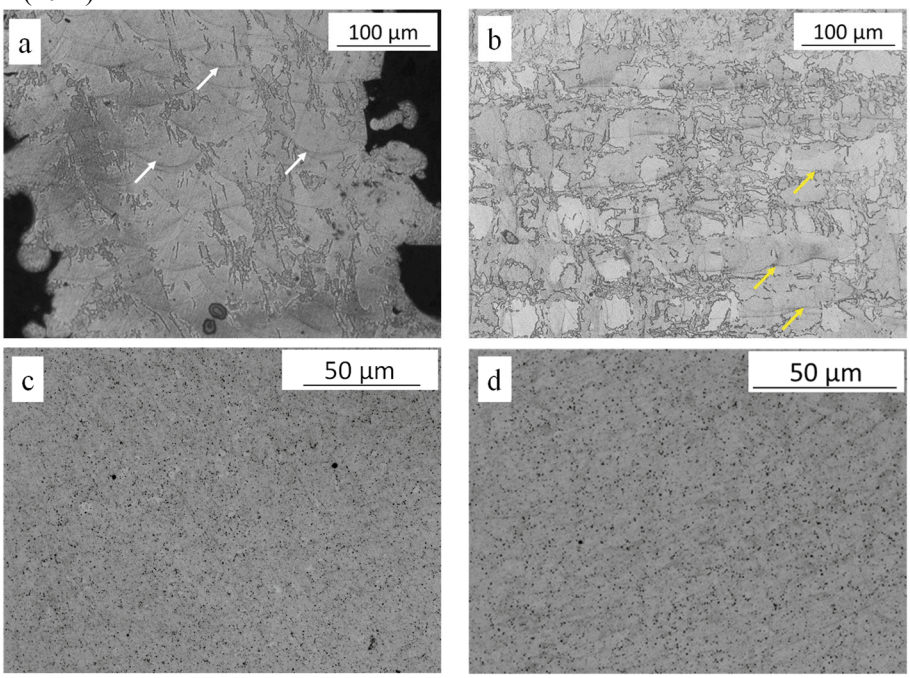

Fig. 3. Optical micrographs of longitudinal (a) and transverse (b) cross-sections of AB samples. Melt pools, scan tracks and columnar grain sections were highlighted by white, yellow, and red arrows, respectively. Optical micrographs of longitudinal (c) and transverse (d) cross-sections of HT samples.

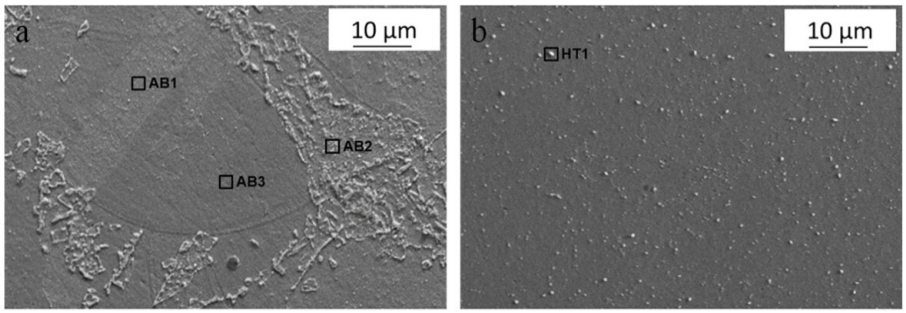

Fig. 4. SEM optical micrographs of cross-section of AB (a) and HT (b) samples.

The microstructure of AB and HT samples was further investigated under SEM. The micrographs at higher magnification of AB and HT samples were reported in Fig. 4a and 4b, respectively. In Fig. 4a, areas of different color highlight the presence of elongated grains. EDS analyses (spectrum AB1 and AB3 in Table 4) reveal a chemical composition close to the nominal composition of the alloy. Lighter particles are also visible, which resulted to be

particularly rich in Cu (spectrum AB2 in Table 4). These are likely segregations rich in Cu formed during the rapid solidification as also reported in An et al. (2023a).

During the heat treatment these segregations are dissolved, and this promotes the formation of Cu-rich precipitates along the grain boundaries and within the matrix, clearly visible in Fig. 4b. The presence of Cu was demonstrated by EDS results for HT1 spectrum in Fig. 4b and Table 4.

Table 4. Chemical elements measured by EDS (all results in weight%).

Spectrum	*Si*	*Mn*	*Cr*	*Fe*	*Ni*	*Cu*
AB1	0.95	-	17.61	71.39	5.21	4.84
AB2	-	-	13.62	57.99	3.96	**24.42**
AB3	0.99	1.01	17.26	72.26	4.69	3.79
HT1	-	-	11.96	48.19	3.44	**36.41**

3.3. Micro hardness

The hardness of AB samples was 345 ± 10 HV, while for HT samples a hardness of 495 ± 11 HV was measured. The HT samples shown an increase of 45% of hardness compared to the AB samples. In accordance with Garcia-Cabezon et al. (2022) the recrystallization of the structure and the Cu-rich precipitates formed during aging treatment were responsible for the increase in hardness.

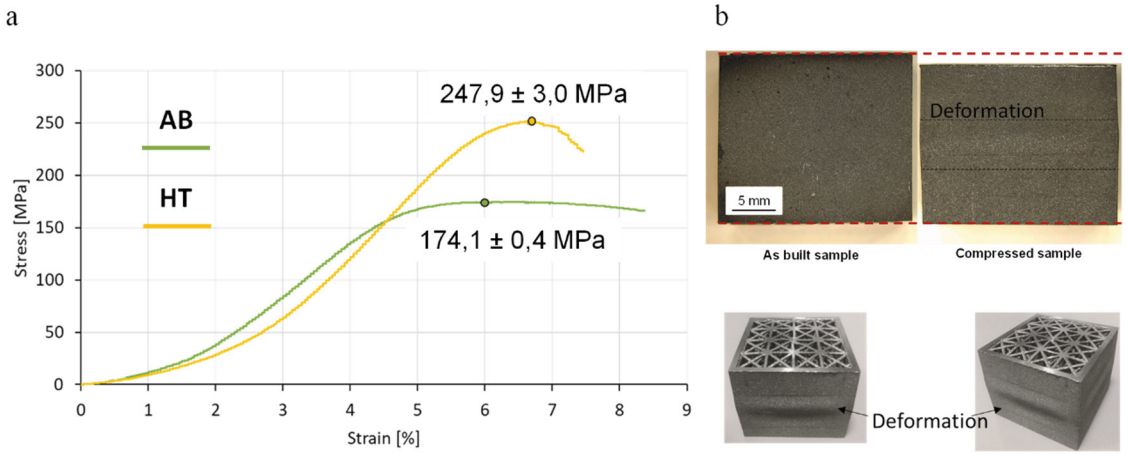

Fig. 5. (a) Stress-strain curves of AB and HT samples. (b) samples before and after compression test.

3.4. Mechanical characterizations

Compression tests were performed on the AB and HT samples. The stress-strain curves calculated from the compression test are shown in Fig. 5a.

A different behavior for the AB and HT samples was detected. In particular, the HT samples exhibited higher strength compared to the AB samples, reaching higher ultimate strength (σ_M). The σ_M of AB samples was 174.1 ± 0.4 MPa, while for the HT samples this value increased of 42% reaching 247.9 ± 3.0 MPa. Moreover, AB samples showed a plateau (typical of bending-dominated behavior, which exhibited good absorption properties, ideal for shock absorption applications Jin et al. (2021); Kotzem et al. (2023)) after reaching the maximum stress and they did not present a collapse point. The stress measured during compression tests of HT samples grew up to the ultimate strength (σ_M) and decreased immediately after. The higher stress corresponds to the buckling of the central “floor” of the

structure as shown in Fig. 5b. After buckling phenomena, the deformation of the struts continued. The load decreased because some of the struts were deformed and broken, and the deformation of the entire structure was easier.

A complete overview of mechanical characteristics is reported in Table 5. The Young's modulus of HT was 64.2 ± 1.9 GPa, 30% higher than the AB samples which was 49.5 ± 0.0 GPa. The yield stress of HT was 237.7 ± 6.8 MPa, 44% higher than the AB samples which was 165.3 ± 4.0 MPa. After the tests, the deformation of AB and HT samples were 0.84 mm and 0.33 mm, respectively. The stiffness, yield stress and ultimate strength increased after the heat treatment, as already discussed by Y. Si Mo et al. Yeon et al. (2022).

The HT samples exhibited higher stiffness, hardness and strength probably due to the homogenization and recrystallization of the microstructure. In particular, the formation of Cu-rich precipitates (Fig. 3c-d) gives higher isotropy and ductility Lashgari et al. (2020).

Table 5. Chemical elements measured by EDS. All results in weight%.

	AB	**HT**
E [GPa]	49.5 ± 0.0	64.2 ± 1.9
σ_y [MPa]	165.3 ± 4.0	237.7 ± 6.8
ε_y [%]	4.9 ± 0.1	6.2 ± 0.4
σ_M [MPa]	174.1 ± 0.4	247.9 ± 3.0
ε_M [%]	6.1 ± 0.6	6.9 ± 0.4

An interesting finding of this work was the behavior of the shell. In fact, the solid part followed the deformation of the structure, as shown in Fig. 5b, and no detachment of the shell from the lattice occur under compression.

This is interesting since a detachment of the shell during the compression test can be expected due to the expansion of the structure in the lateral direction. This can be encouraged by the presence of defect at the shell/lattice interface. Instead, the interface connection of 17-4PH structures was stronger and the detachment of the shell did not occur.

The struts after compression test are reported in Fig. 6. It can be noticed that the broken struts highlighted with the white arrows are in the center part of lattice, while the struts connected to the shell were not compromised. To better understand the behavior of the struts within the structure a deeper analysis is required. Based on the observed mechanical behavior, shock absorption can be considered as a possible application for these kinds of structures.

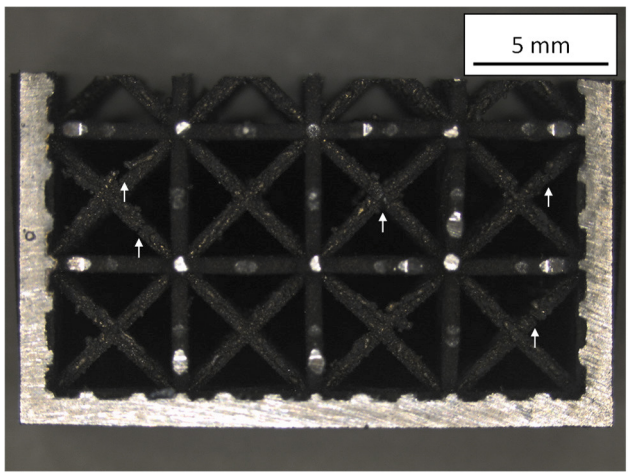

Fig. 6. Examples of strut after compression test (a) connected to the shell and (b) in the center part of the lattice samples.

4. Conclusions

The aim of this work was to analyze the behavior of 17-4 PH lattice samples surrounded by a solid shell, manufactured by L-PBF technology. In fact, lattices are often integrated in a solid structure in actual component and these complex structures require a proper characterization, considering in particular the critical feature represented by the lattice/shell interface. The lattice part with a cubic-based geometry was designed with FCC unit cell and a solid shell was built around the structure. Moreover, a solution treatment followed by ageing was performed. The microstructure was investigated, and compression tests were carried out to analyze the mechanical properties. It can be concluded that:

- As built and heat-treated samples exhibited different microstructure, hardness, and mechanical properties. As a consequence of the heat treatment, the results indicated that the HT samples exhibited higher stiffness and strength, better supporting the load, compared to the AB samples.
- The homogenization of the microstructure occurred due to the solution treatment, while the formation of strengthening Cu-rich precipitates was due to the aging treatment, as well as strength and hardness increase.
- Defects were detected at the interface between lattice and solid part, such as porosities. However, the shell did not detach from the internal lattice part during compression tests but followed the collapse of the internal lattice.

In this study the shell help to better support the load and follows the collapse of the internal lattice structure. Shock absorption can be considered as the possible applications of 17-4 PH lattice structure, but further studies are needed to better understand the failure mechanism under compression.

Acknowledgements

Financed by the European Union - NextGenerationEU (National Sustainable Mobility Center CN00000023, Italian Ministry of University and Research Decree n. 1033 - 17/06/2022, Spoke 11 - Innovative Materials & Lightweighting-CUP: D83C22000690001).

The Authors deeply thank MSc.Eng. G. Valsecchi from TAV Vacuum Furnaces Spa for heat treatment of samples and Dr. L. Montesano for support in SEM analysis.

References

An, Sohee, Du Rim Eo, Il Sohn, and Kyunsuk Choi. 2023a. “Homogenization on Solution Treatment and Its Effects on the Precipitation-Hardening of Selective Laser Melted 17-4PH Stainless Steel.” *Journal of Materials Science and Technology* 166:47–57. doi: 10.1016/j.jmst.2023.04.055.

An, Sohee, Du Rim Eo, Il Sohn, and Kyunsuk Choi. 2023b. “Homogenization on Solution Treatment and Its Effects on the Precipitation-Hardening of Selective Laser Melted 17-4PH Stainless Steel.” *Journal of Materials Science and Technology* 166:47–57. doi: 10.1016/j.jmst.2023.04.055.

Bai, Long, Cheng Gong, Xiaohong Chen, Jia Zheng, Liming Xin, Yan Xiong, Xiaoying Wu, Mingjin Hu, Kun Li, and Yuanxi Sun. 2021. “Quasi-Static Compressive Responses and Fatigue Behaviour of Ti-6Al-4 V Graded Lattice Structures Fabricated by Laser Powder Bed Fusion.” *Materials and Design* 210:110110. doi: 10.1016/j.matdes.2021.110110.

Bayat, Mohamad, Aditi Thanki, Sankhya Mohanty, Ann Witvrouw, Shoufeng Yang, Jesper Thorborg, Niels Skat Tiedje, and Jesper Henri Hattel. 2019. “Keyhole-Induced Porosities in Laser-Based Powder Bed Fusion (L-PBF) of Ti6Al4V: High-Fidelity Modelling and Experimental Validation.” *Additive Manufacturing* 30(July):100835. doi: 10.1016/j.addma.2019.100835.

Bertocco, Alcide, Gianluca Iannitti, Antonio Caraviello, and Luca Esposito. 2022. “Lattice Structures in Stainless Steel 17-4PH Manufactured via Selective Laser Melting (SLM) Process: Dimensional Accuracy, Satellites Formation, Compressive Response and Printing Parameters Optimization.” *International Journal of Advanced Manufacturing Technology* 120(7–8):4935–49. doi: 10.1007/s00170-022-08946-2.

Bertol, Liciane Sabadin, Wilson Kindlein Júnior, Fabio Pinto da Silva, and Claus Aumund-Kopp. 2010. “Medical Design: Direct Metal Laser Sintering of Ti-6Al-4V.” *Materials and Design* 31(8):3982–88. doi: 10.1016/j.matdes.2010.02.050.

Cantaboni, Francesco, Paola S. Ginestra, Marialaura Tocci, Andrea Avanzini, Elisabetta Ceretti, and Annalisa Pola. 2022. “Compressive Behavior of Co-Cr-Mo Radially Graded Porous Structures under as-Built and Heat-Treated Conditions.” *Frattura Ed Integrita Strutturale* 16(62):490–504. doi: 10.3221/IGF-ESIS.62.33.

Dong, Guoying, Yunlong Tang, Dawei Li, and Yaoyao Fiona Zhao. 2020a. “Design and Optimization of Solid Lattice Hybrid Structures Fabricated

by Additive Manufacturing." *Additive Manufacturing* 33(February):101116. doi: 10.1016/j.addma.2020.101116.
Dong, Guoying, Yunlong Tang, Dawei Li, and Yaoyao Fiona Zhao. 2020b. "Design and Optimization of Solid Lattice Hybrid Structures Fabricated by Additive Manufacturing." *Additive Manufacturing* 33(February):101116. doi: 10.1016/j.addma.2020.101116.
Fu, Jin, Junhao Ding, Shuo Qu, Lei Zhang, Michael Yu Wang, M. W. Fu, and Xu Song. 2022. "Improved Light-Weighting Potential of SS316L Triply Periodic Minimal Surface Shell Lattices by Micro Laser Powder Bed Fusion." *Materials and Design* 222. doi: 10.1016/j.matdes.2022.111018.
Garcia-Cabezon, C., M. A. Castro-Sastre, A. I. Fernandez-Abia, M. L. Rodriguez-Mendez, and F. Martin-Pedrosa. 2022. "Microstructure–Hardness–Corrosion Performance of 17–4 Precipitation Hardening Stainless Steels Processed by Selective Laser Melting in Comparison with Commercial Alloy." *Metals and Materials International* 28(11):2652–67. doi: 10.1007/s12540-021-01155-8.
Ginestra, P. S., L. Riva, G. Allegri, L. Giorleo, A. Attanasio, and E. Ceretti. 2020. "Analysis of 3D Printed 17-4 PH Stainless Steel Lattice Structures with Radially Oriented Cells." *Industry 4.0 – Shaping The Future of The Digital World* 136–41. doi: 10.1201/9780367823085-25.
Jin, Nan, Zhenyu Yan, Yangwei Wang, Huanwu Cheng, and Hongmei Zhang. 2021. "Effects of Heat Treatment on Microstructure and Mechanical Properties of Selective Laser Melted Ti-6Al-4V Lattice Materials." *International Journal of Mechanical Sciences* 190(July 2020):106042. doi: 10.1016/j.ijmecsci.2020.106042.
Kareem, Mohammed Qasim, Tamás Mikó, Gréta Gergely, and Zoltán Gácsi. 2023. "A Review on the Production of 17-4PH Parts Using Press and Sinter Technology." *Science Progress* 106(1):1–31. doi: 10.1177/00368504221146060.
Kotzem, Daniel, Tizian Arold, Kevin Bleicher, Rajevan Raveendran, Thomas Niendorf, and Frank Walther. 2023. "Ti6Al4V Lattice Structures Manufactured by Electron Beam Powder Bed Fusion - Microstructural and Mechanical Characterization Based on Advanced in Situ Techniques." *Journal of Materials Research and Technology* 22(January 2023):2111–30. doi: 10.1016/j.jmrt.2022.12.075.
Lashgari, H. R., C. Kong, E. Adabifiroozjaei, and S. Li. 2020. "Microstructure, Post Thermal Treatment Response, and Tribological Properties of 3D Printed 17-4 PH Stainless Steel." *Wear* 456–457. doi: 10.1016/j.wear.2020.203367.
Leo, Paola, Marcello Cabibbo, Antonio Del Prete, Sara Giganto, Susana Martínez-Pellitero, and Joaquin Barreiro. 2021. "Laser Defocusing Effect on the Microstructure and Defects of 17-4ph Parts Additively Manufactured by Slm at a Low Energy Input." *Metals* 11(4). doi: 10.3390/met11040588.
Mahmoudi, Mohamad, Alaa Elwany, Aref Yadollahi, Scott M. Thompson, Linkan Bian, and Nima Shamsaei. 2017. "Mechanical Properties and Microstructural Characterization of Selective Laser Melted 17-4 PH Stainless Steel." *Rapid Prototyping Journal* 23(2):280–94. doi: 10.1108/RPJ-12-2015-0192.
Razavi, Seyed Mohammad Javad, Andrea Avanzini, Giovanna Cornacchia, Luca Giorleo, and Filippo Berto. 2021. "Effect of Heat Treatment on Fatigue Behavior of As-Built Notched Co-Cr-Mo Parts Produced by Selective Laser Melting." *International Journal of Fatigue* 142(August 2020):105926. doi: 10.1016/j.ijfatigue.2020.105926.
Wu, Ziheng, Sneha Prabha Narra, and Anthony Rollett. n.d. "Exploring the Fabrication Limits of Thin-Wall Structures in a Laser Powder Bed Fusion Process." doi: 10.1007/s00170-020-05827-4/Published.
Xiao, Zefeng, Yongqiang Yang, Ran Xiao, Yuchao Bai, Changhui Song, and Di Wang. 2018. "Evaluation of Topology-Optimized Lattice Structures Manufactured via Selective Laser Melting." *Materials and Design* 143:27–37. doi: 10.1016/j.matdes.2018.01.023.